

# STELLAR-CHROMOSPHERIC MODELS

Eugene H. Avrett

*Smithsonian Institution  
Astrophysical Observatory*

## ABSTRACT

In "Types of Theoretical Models" we describe two basic types of theoretical models — radiative equilibrium and empirical — that are used to represent stellar chromospheres. The next Section is a summary of recent work on the construction of radiative-equilibrium model atmospheres that show an outward temperature increase in the surface layers. Also, we discuss the chromospheric cooling due to spectral lines. In "Solar Empirical Models" we describe the empirical determination of solar-type chromospheric models that, in order to match observations, imply a temperature rise substantially greater than that predicted by radiative equilibrium. Such a temperature rise must be largely due to mechanical heating. An attempt is made in the concluding Section to apply a scaled solar chromospheric model to a star with a different surface gravity. The results suggest that the chromospheric optical thickness is sensitive to gravity and that the width of chromospheric line emission increases with stellar luminosity, in qualitative agreement with the width-luminosity relationship observed by Wilson and Bappu.

## TYPES OF THEORETICAL MODELS

Current research on chromospheric models can be described in terms of two different approaches. The first involves calculating a theoretical spectrum on the basis of a set of *a priori* assumptions that includes the assumption of radiative equilibrium. Often a grid of such models is constructed for different values of effective temperature, surface gravity, and composition. The calculation of radiative-equilibrium models has reached a new level of sophistication recently with the detailed inclusion of non-LTE effects (Auer and Mihalas, 1972) and line blanketing (Kurucz, Peytremann, and Avrett, 1972).

These models may account for most of the observed features in normal stellar spectra, but they do not account for the chromospheric spectra of late-type stars such as the Sun. As discussed in the following section, the

only point of controversy in the solar case is whether or not radiative equilibrium plays even a minor role in the initial chromospheric temperature rise.

The second approach is the same as the first except that in place of the radiative-equilibrium assumption, which fixes the temperature distribution, we adjust the temperature versus depth by trial and error until the computed spectrum agrees with the observed one. An empirical model for the solar chromosphere is obtained in this way, as discussed below. The solar spectrum has been observed throughout different wavelength regions in such detail that we can test our theoretical models for consistency: Typically, we have a greater number of spectral features to match than parameters to adjust.

Once a detailed empirical chromospheric model is obtained for the Sun, or for any well-observed star, it is possible to calculate the mechanical energy flux as a function of depth, i.e., the amount that must be added to the radiative flux to make the total flux constant with depth. A knowledge of the mechanical flux distribution should lead us to an understanding of the nonradiative heating mechanism, and then perhaps to a method by which this flux distribution can be calculated for any star. As a result, we would be able to construct realistic chromospheric models based on the assumption of radiative equilibrium with mechanical heating. Despite the work still to be done, this goal seems within reach.

## RADIATIVE-EQUILIBRIUM MODELS

Here we summarize recent work on the construction of model atmospheres in radiative equilibrium that show an outward temperature increase in the surface layers.

Auer and Mihalas (1969a, b, 1970) have calculated non-LTE radiative-equilibrium model atmospheres for hot stars with effective temperatures of  $12500^\circ$  and  $15000^\circ\text{K}$ . They examine the heating of the outer layers caused by a positive flux derivative in various continuum wavelength intervals when  $J_\nu$  exceeds the continuum source function. They find that the main source of heating is due to photoionization in the Balmer continuum and that this is mostly a population effect: The  $H\alpha$  line provides an efficient channel for 3 to 2 transitions causing a greater level 2 population, greater heating, and a surface temperature rise. The line itself tends to cool the atmosphere, but by an amount smaller than the heating caused by the change of level populations.

Feautrier (1968) also computed non-LTE model atmospheres in radiative and hydrostatic equilibrium with effective temperatures  $15000^\circ$  and

25000°K and  $\log g = 4$ , and with a solar effective temperature together with both  $\log g = 2$  and solar gravity. He includes departures from LTE in  $H^-$  as well as in hydrogen. In the higher effective-temperature atmospheres, he finds surface-temperature increases of as much as 1000° or 2000°K in agreement with Auer and Mihalas, but in the solar effective-temperature cases, he finds increases of only a few hundred degrees.

The physical mechanism responsible for the surface-temperature rise was pointed out by Cayrel (1963); it is an extension of the classical radiative-equilibrium model of a planetary nebula, as discussed, for example, by Baker, Menzel, and Aller (1938). Essentially, there is a shift from LTE in the underlying star to unbalanced radiative equilibrium in the low-density outer atmosphere, where the temperature is close to the color temperature of the star, rather than to the lower classical boundary temperature.

Skumanich (1970) has recently discussed the validity of the Cayrel mechanism in response to an earlier suggestion by Jordan (1969) that radiative equilibrium is incompatible with a departure of the continuum source function from the Planck function for atmospheres of large  $H^-$  concentration.

Gebbie and Thomas (1970, 1971) discuss the role that collisions play in the energy balance. They find that the low chromospheric densities are too high to be neglected in calculating the temperature and atomic populations. Hence, the planetary-nebula type of calculation does not give correct results for the low chromosphere. They discuss the determination of the temperature distribution in terms of transfer effects and population effects and, as a measure of population effects, introduce a quantity they call the "temperature control bracket," defined as the photoionization rate divided by the corresponding integral containing the monochromatic source function instead of  $J_\nu$ .

Most of the above studies are concerned with heating due to photoionization. A number of other recent studies have been made of radiative-energy losses and of cooling due mainly to lines.

Dubov (1965) emphasizes that the main factor responsible for the cooling of the chromosphere is radiation in separate spectral lines. Athay (1966) discusses the energy loss from the middle chromosphere due to the hydrogen Balmer lines. Frisch (1966) estimates the cooling due to collisional excitation in various lines and finds that, in the vicinity of the temperature minimum, the energy losses due to the Ca and Mg H and K resonance lines together with the Ca infrared triplet are approximately half those due to radiative recombination. Athay and Skumanich (1969)

and Athay (1970) carry out extensive non-LTE line-blanketing calculations and find that the tendency for the temperature to rise in the surface layers due to the Cayrel mechanism is strongly resisted by the effects of line blanketing; they also find that a chromospheric rise of  $300^\circ$  or more would require a substantial input of mechanical energy.

Hence, it is by no means certain that even the initial temperature rise in the low solar chromosphere occurs as a consequence of radiative equilibrium.

## SOLAR EMPIRICAL MODELS

In this section we discuss the empirical determination of model chromospheres, such as that of the Sun, for which the temperature rise is substantially greater than that predicted by radiative-equilibrium calculations. The results shown here are from the study of Linsky and Avrett (1970) of the solar H and K lines. The model has been chosen such that the predicted microwave spectrum lies within observed limits and the computed H- and K-line profiles resemble those observed from quiet regions near the center of the solar disk. This model is intended to be only a representative one. Empirical solar models that also match various features in the extreme ultraviolet have been constructed more recently by Noyes and Kalkofen (1970), Gingerich, Noyes, Kalkofen, and Cuny (1971), and Vernazza, Avrett, and Loeser (1972).

Disk-center brightness temperatures observed in the region  $10\mu$  to 2 cm are shown in Figure I-5. The solar continuous opacity increases with increasing wavelength in this region, so that radiation at longer wavelengths is emitted by layers at greater heights in the atmosphere. The spectrum shortward of about  $300\mu$  originates in the photosphere, and that longward, in the chromosphere.

The solid line in Figure I-5 represents the brightness temperatures we computed based on the temperature-height distribution shown in Figure I-6. The abrupt temperature increase that begins at about  $7500^\circ$  has been introduced to account for the Lyman-continuum spectrum shortward of  $912 \text{ \AA}$  and to keep the computed gas pressure above coronal values (see Athay, 1969, Noyes and Kalkofen, 1970).

Unfortunately, there is a second function of height that must be introduced in order to specify the model. In our study of the calcium lines, we need to introduce non-thermal Doppler broadening to explain the observed central line widths. The line absorption coefficient at the wavelength  $\lambda$  for an atom of mass  $M$  has the Doppler width

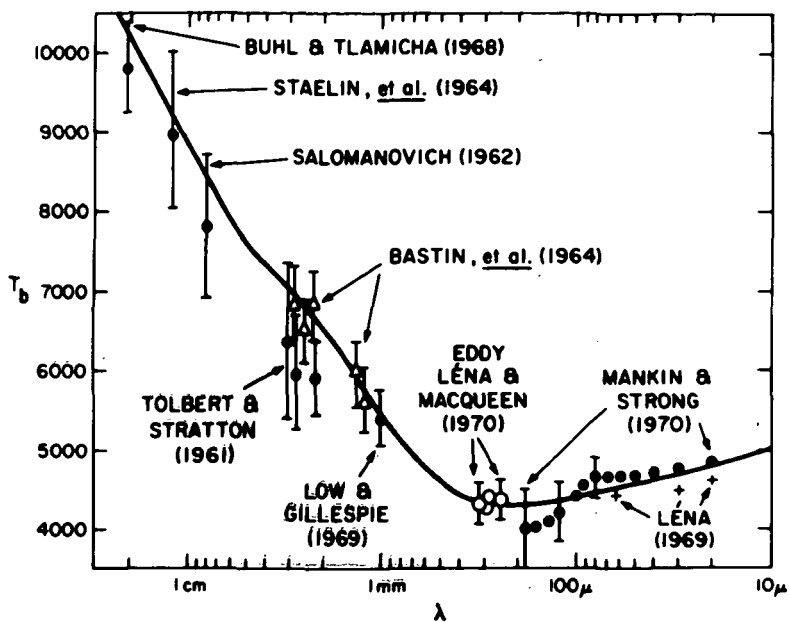


Figure I-5 Comparison of the observed and calculated brightness temperatures of the disk center. References to the papers indicated in the figure are given by Linsky and Avrett (1970).

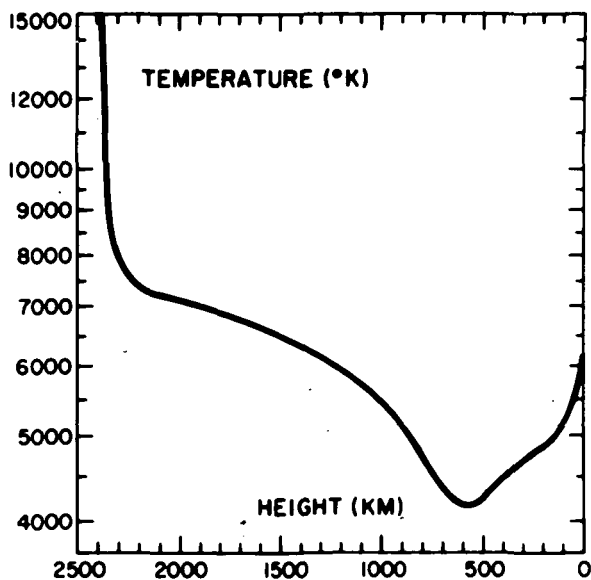


Figure I-6 The assumed temperature-height distribution.

$$\Delta\lambda_D = \frac{\lambda}{c} \sqrt{\frac{2kT}{M} + V^2} ,$$

where  $T$  is the temperature at the given depth. We use the parameter  $V$  as a measure of any required nonthermal Doppler broadening. Central profiles of the Ca II infrared triplet lines, formed between 500 and 1000 km, indicate values of  $V$  in the range 2 to 3 km/sec. Higher in the atmosphere, where the H- and K-line centers are formed,  $V$  must exceed 4 km/sec. We have attempted to adjust  $V(h)$  to obtain good agreement between the calculated and the observed line profiles. The result is shown in Figure I-7.

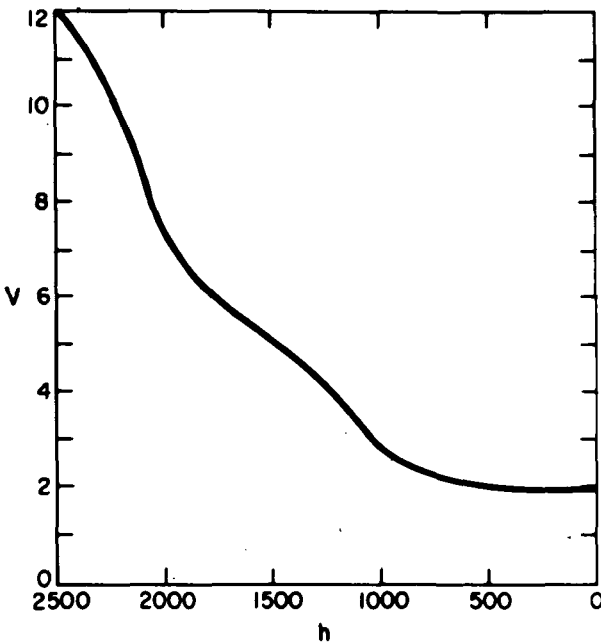


Figure I-7 The nonthermal velocity distribution used in line broadening and in the pressure equation.

We have chosen to use  $V(h)$  also to represent a nonthermal contribution to the total pressure  $P$ . We let

$$P = P_g + \frac{1}{2} \rho V^2 ,$$

where  $P_g$  is the gas pressure and  $\rho$  is the density. This added pressure term extends the model in height and gives better agreement with observed eclipse scale heights.

Given  $T(h)$  and  $V(h)$ , we solve the equations of hydrostatic equilibrium, statistical equilibrium, and radiative transfer for atomic hydrogen, taking into account the ionization and excitation of other constituents as required. Figure I-8 shows the resulting ground-state hydrogen number density  $n_1$ , the electron and proton densities  $n_e$  and  $n_p$ , the electron pressure  $P_e$ , the total pressure  $P$ , and the turbulent pressure  $P_t = 1/2\rho V^2$ .

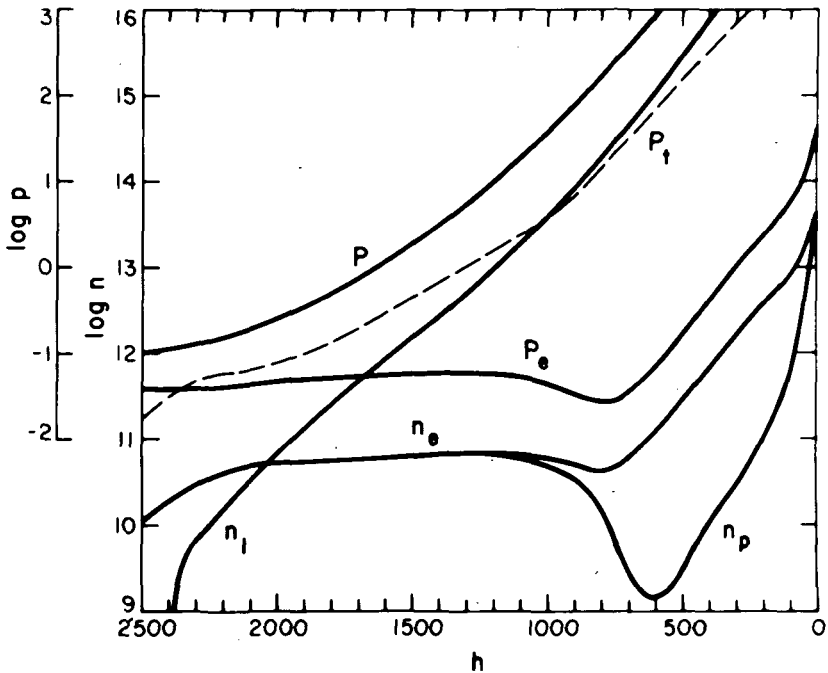


Figure I-8 Distributions of pressure and number density, including  $n_e$  the electron density,  $n_p$  the proton density,  $n_1$  the density of hydrogen atoms in the ground state,  $P_e$  the electron pressure,  $P_t$  the turbulent pressure, and  $P$  the total pressure.

Having established the atmospheric model, we solve the transfer and statistical-equilibrium equations for Ca II. Figure I-9 shows the computed frequency-independent source function for the K line plotted against height and against line-center optical depth. This source function is a measure of the ratio of upper and lower level number densities. If this

ratio were given by the Boltzmann equation, as in LTE,  $S$  would be equal to the Planck function  $B$ , which is also shown for comparison.

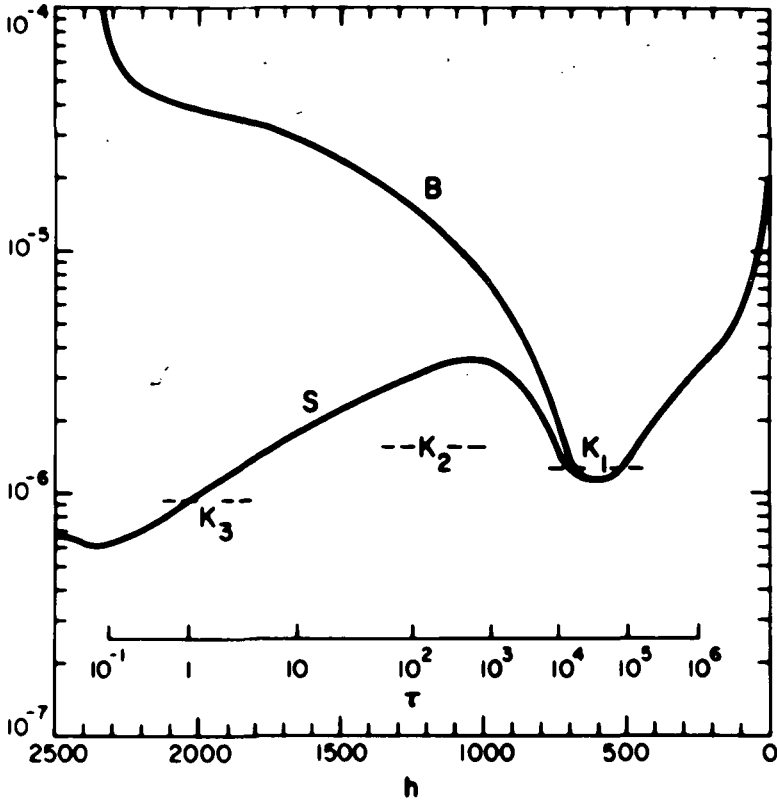


Figure I-9 The K-line source function, Planck function, and line-center optical depth. The computed line-intensity values at  $K_1$ ,  $K_2$ , and  $K_3$  are indicated by dashed lines.

The computed H- and K-line intensity profiles for the center of the solar disk are shown in Figure I-10, compared with those observed by White and Suemoto (1968). We plot the average of the red and violet halves of each observed profile. Residual intensities are plotted in Figure I-10, but the absolute intensities of  $K_1$ ,  $K_2$ , and  $K_3$  (the minimum, peak, and central values) are shown for reference in Figure 5. The  $K_2$  peak intensity is substantially less than the maximum of  $S$  because of the Doppler-width variation with height in this region. The agreement between calculated and observed profiles shown in Figure 6 is the best we obtained after many trial adjustments of  $T(h)$  and  $V(h)$ .

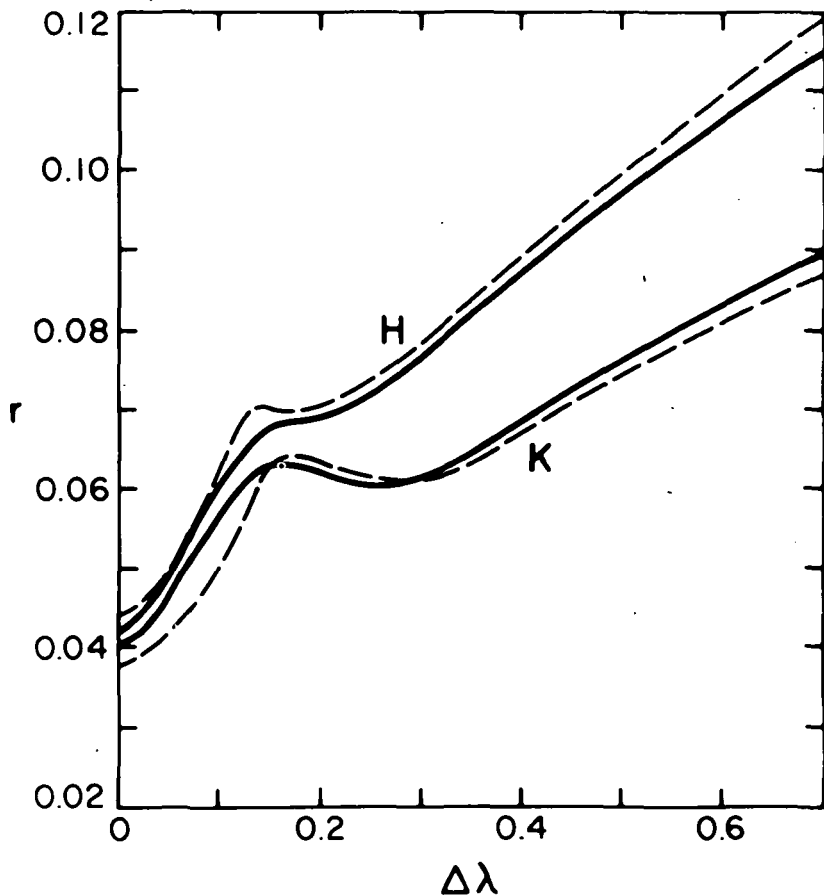


Figure I-10 The computed disk-center H- and K-line profiles (broken lines) compared with the corresponding observed profiles of White and Suemoto (1968), (solid lines).

These emergent line profiles are calculated assuming that the monochromatic line source function  $S_\nu$  is equal to  $S$  throughout the line. This assumption is valid in the line core, where Doppler redistribution takes place, and in the far wings, where  $S = S_\nu = B$ . In the intermediate wings, several Doppler widths from line center, the situation is unclear. In this region the coherent-scattering approximation  $S_\nu = J_\nu$  may be more accurate; if so, the computed line profile may have a different shape between  $K_2$  and  $K_1$ .

The quiet-Sun  $K_2$  emission peaks are weak and subject to various fluctuations from point to point on the disk. It may be that we should

try to match not the spatially averaged profiles shown in Figure I-10, but the ones observed with high spatial resolution.

It is of interest to note the difference in shape between the quiet-Sun H and K profiles shown in Figure I-11 and the plage profiles in Figure I-12. The question of whether  $S_{\nu}$  is closer to S or  $J_{\nu}$  in the intermediate line wings might be answered by a theoretical study of plage profiles. The published research on coherence and noncoherence in the K-line wings is discussed in Section III.2 of the review by Linsky and Avrett (1970).

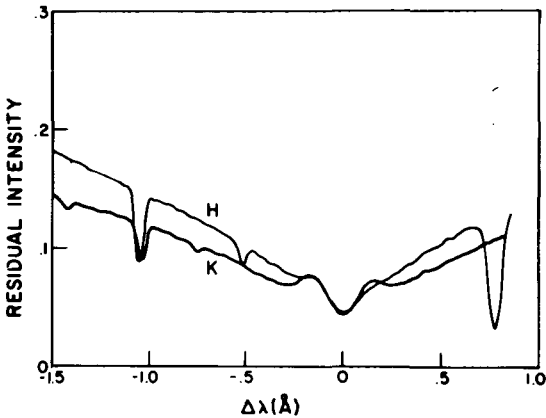


Figure I-11 Low-spatial-resolution residual intensities of the H and K lines for quiet regions near the disk center, as obtained by Linsky (1970). Although the K line exhibits a distinct double reversal, the H line exhibits only a plateau in the violet wing and no reversal at all in the red wing.

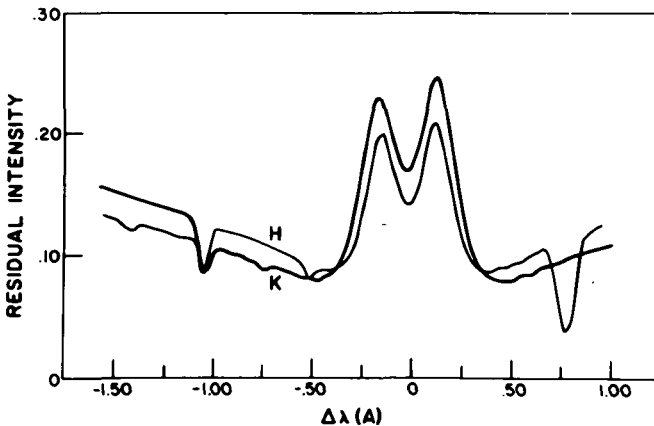


Figure I-12 Low-spatial-resolution residual intensities of the H and K lines for a plage region, as obtained by Linsky (1970).

## THE EFFECT OF GRAVITY ON CHROMOSPHERIC THICKNESS

In this final section we attempt to apply a scaled solar chromospheric model to a star having a different surface gravity. Figure I-13 shows the solar temperature distribution to be used for this purpose. This  $T(h)$  differs somewhat from the earlier one shown in Figure I-6 because we have made changes in the corresponding  $V(h)$ . The photospheric temperature distribution from zero height ( $\tau_{5000} = 1$ ) to the temperature minimum is approximately in radiative equilibrium. The right-hand portion of Figure I-14 shows the calculated photospheric temperature distribution for a star with a solar effective temperature but with  $\log g = 2$ . The  $\log g = 2$  photosphere is more extended in height by a factor of about 250, which is approximately the ratio of the two values of  $g$ . We have arbitrarily chosen a chromosphere for this star that is scaled from the solar model by roughly the same height factor. Note that the calculated chromospheric  $\tau_{5000}$  scale is very different in the two cases. The computed number densities are shown in Figure I-15: Those for  $\log g = 2$  are about a factor of 10 smaller than the corresponding solar values. However, the  $\log g = 2$  scale height exceeds that of the Sun by the much larger factor 250. Whenever the opacity is proportional to  $n_H$ , as it is for the K line, we expect the  $\log g = 2$  chromosphere to have a greater optical thickness.

The K-line source function and line-center optical depth for the two cases are shown in Figure I-16. In this figure and in the preceding one, the  $\log g = 2$  height scale appears at the top and the solar height scale at the bottom. Note that at the temperature minimum,  $\tau_K$  for  $\log g = 2$  is an order of magnitude greater than  $\tau_K(\text{solar})$ . This increased thickness leads to a greater width of that portion of the line that originates above the temperature minimum. When the thickness is greater, we need to look farther out in the line wings to see the photosphere. Figure I-17 shows the two computed flux profiles.

These results illustrate a plausible effect of a change in gravity: The lower-gravity atmosphere is less dense but geometrically extended to a greater degree. The outer layers then have greater optical thickness, which leads to a greater line-emission width and the geometrically extended atmosphere tends to have a greater luminosity. Hence, the width  $W$  increases with luminosity  $L$ . The degree to which these results appear consistent with the observed relationship  $W \propto L^{1/6}$  found by Wilson and Bappu (1957) will be discussed later at this meeting by Dr. E. Peytremann.

Further attention should be given to the shape of the computed profiles shown in Figure I-17. The observed stellar profiles appear to have a

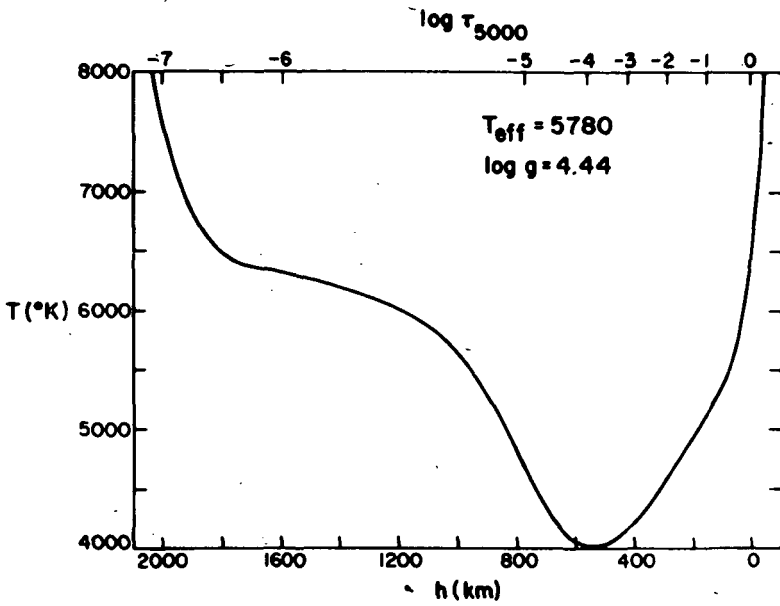


Figure I-13 The solar,  $\log g = 4.44$ , temperature distribution used for comparison with another case for which  $\log g = 2$ .

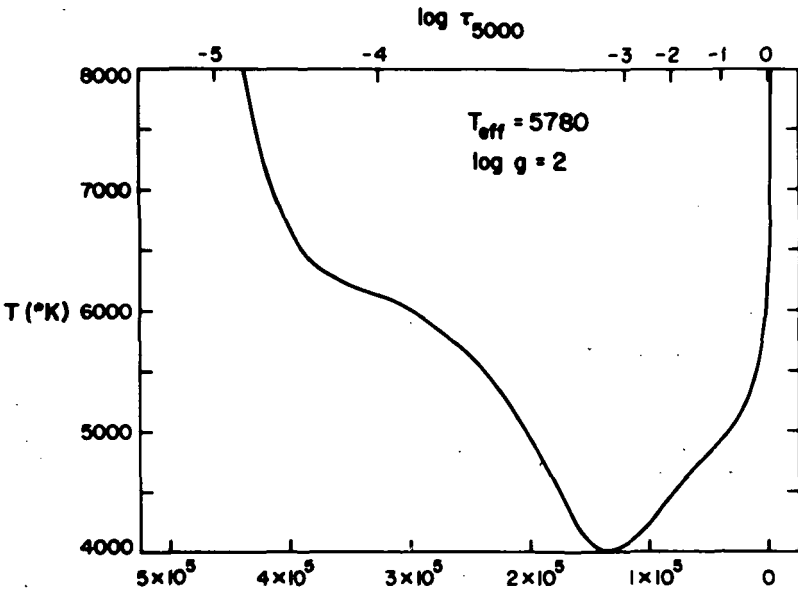


Figure I-14 The adopted  $\log g = 2$  temperature distribution.

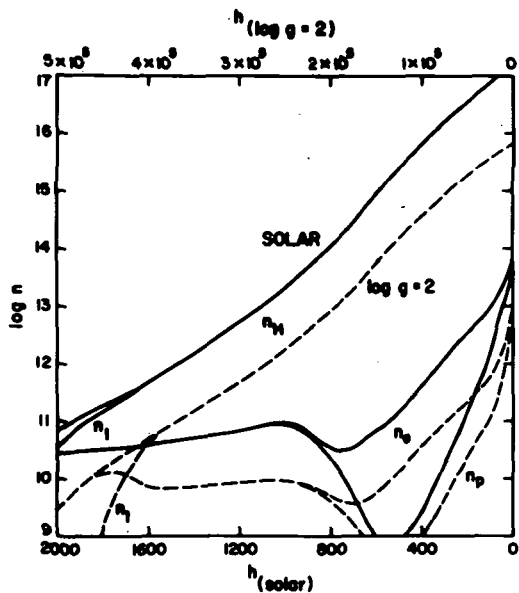


Figure 15 A comparison of the number densities in the two cases.

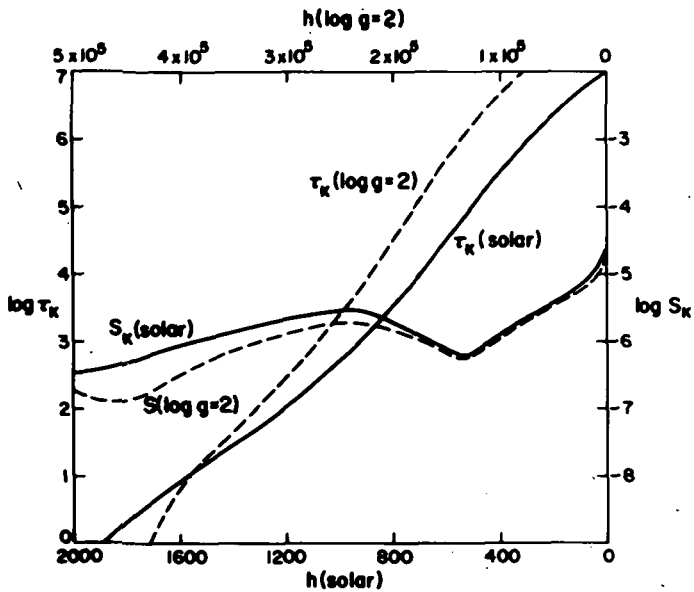


Figure 16 The K line source function and line-center optical depth in the two cases.

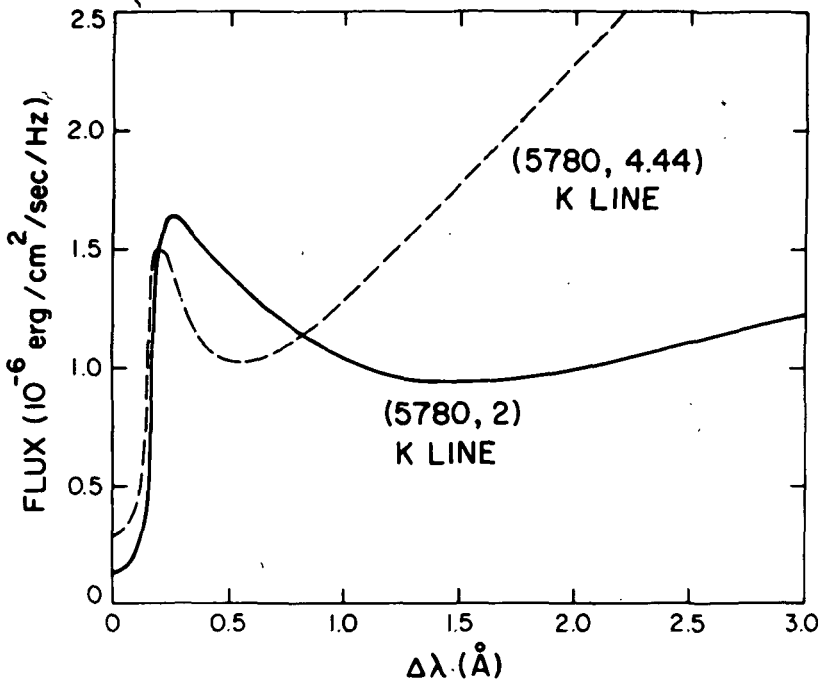


Figure I-17 The computed flux profile for the K line in the two cases.

sharper transition between the  $K_2$  emission peak and the  $K_1$  minimum (see, for example, Griffin, 1968, and Liller, 1968). Perhaps the transition between Doppler core and damping wings should occur farther out in the line. Also, as noted in the last section, we should examine the effects of *partial coherence in the region between  $K_2$  and  $K_1$* .

## REFERENCES

- Athay, R.G. 1966, *Astrophys. J.*, **146**, 223.  
 Athay, R.G. 1969, *Solar Phys.*, **9**, 51.  
 Athay, R.G. 1970, *Astrophys. J.*, **161**, 713.  
 Athay, R.G., Skumanich, A. 1969, *Astrophys. J.*, **155**, 273.  
 Auer, L.H., Mihalas, D. 1969a, *Astrophys. J.*, **156**, 157.  
 Auer, L.H., Mihalas, D. 1969b, *Astrophys. J.*, **156**, 681.  
 Auer, L.H., Mihalas, D. 1970, *Astrophys. J.*, **160**, 233.  
 Auer, L.H., Mihalas, D. 1972, *Astrophys. J. Suppl.*, **24**, 193.  
 Baker, J.G., Menzel, D.H., Aller, L.H. 1938, *Astrophys. J.*, **88**, 422.  
 Cayrel, R., 1963, *Comptes Rendus*, **257**, 3309.  
 Dubov, E.E., 1965, *Soviet Astron. - A.J.*, **9**, 782.

- Feautrier, P. 1968, *Ann. D'Astrophys.*, **31**, 257.
- Frisch, H. 1966, *J. Quant. Spectrosc. Radiat. Transfer*, **6**, 629.
- Gebbie, K.B., Thomas, R.N. 1970, *Astrophys. J.*, **161**, 229.
- Gebbie, K.B., Thomas, R.N. 1971, *Astrophys. J.*, **168**, 461.
- Gingerich, O., Noyes, R.W., Kalkofen, W., Cuny, Y. 1971, *Solar Phys.*, **18**, 347.
- Griffin, R.F. 1968, *A Photometric Atlas of the Spectrum of Arcturus*, Cambridge Philosophical Society, Cambridge, England.
- Jordan, S.D. 1969, *Astrophys. J.*, **157**, 465.
- Kurucz, R.L., Peytremann, E., Avrett, E.H. 1972, *Line Blanketed Model Atmospheres for Early Type Stars*, U.S. Govt. Printing Office (in press)
- Liller, W. 1968, *Astrophys. J.*, **151**, 589.
- Linsky, J.L. 1970, *Solar Phys.*, **11**, 355.
- Linsky, J.L., Avrett, E.H. 1970, *Publ. Astron. Soc. Pacific*, **82**, 169.
- Noyes, R.W., Kalkofen, W. 1970, *Solar Phys.*, **15**, 120.
- Skumanich, A. 1970, *Astrophys. J.*, **159**, 1077.
- Vernazza, J.E., Avrett, E.H., Loeser, R. 1972, submitted to *Astrophys. J.*
- White, O.R., Suemoto, Z. 1968, *Solar Phys.*, **3**, 523.
- Wilson, O.C., Bappu, M.K.V. 1957, *Astrophys. J.*, **125**, 661.

#### DISCUSSION FOLLOWING THE INTRODUCTORY TALK BY AVRETT

**Aller** – I should like to ask about the suggested theoretical one-sixth power relationship between calcium emission width and visual luminosity.

**Avrett** – We find an increased width with decreasing gravity, which in turn is normally associated with an increased luminosity. In the session tomorrow Eric Peytremann will show the results we have to date and how they compare with the Wilson-Bappu relation. To summarize them, the  $\log g = 2$  case with a temperature similar to that of the sun turns out with a reasonable mass determination to fit the Wilson-Bappu relation within the error bars. The only other calculation we have done so far is for an effective temperature of  $6000^\circ$  with  $\log g = 4$ ; the error bars again include the Wilson-Bappu relationship but they are very large. At the moment these results are only schematic. Also our choice of a chromosphere in the non-solar cases was completely arbitrary. We have to see whether we just happened to select chromospheres which give the proper optical thickness for the calcium emission.

**Jefferies** – This is more of a comment than a question. One of the things which bedevils comparison between observation and theory of model atmospheres is, of course, the question of the uniqueness of any derived model. In order to characterize an atmosphere fully one needs to introduce a substantial number of parameters. Because of this, one needs